Lateral and Distal Dose of Proton and Carbon Ion Beams for Tumor Cells Using PHITS Simulation Code

Myat Kay Khaing[1] and Nyein Wint Lwin [2]

Abstract

With the development of particle accelerator design and related accessories, the popularity of charged particle therapy has increased. Most commonly used ions for particle therapy are proton and carbon. In terms of dose distribution and relative biological effectiveness (RBE) value, carbon ion is more favorable for deep-seated radioresistant tumor cells. Moreover, it has small lateral scattering compared with proton. But due to the probability of fragmentation itself, fragmented particles travel beyond targeted volume and deposit energy in normal healthy tissues. Although carbon ion shows fragmentation as drawback, better local control of energy is observed in compared with proton.

Keywords: Charged Particle Therapy, relative biological effectiveness (RBE) value

Introduction

One of the major treatments of cancer is using ionizing radiation to destroy cancer cells which is known as radiation therapy. Radiation therapy can be divided into two groups. The first one is traditional radiation therapy which uses photons to irradiate cancer cell. The other is charged particle therapy in which proton and heavy ion are used. Usage of proton to destroy cancer cells is firstly proposed by Robert Wilson at Harvard in 1946 [1]. The basic principle of radiation therapy is to give enough energy to the target tumor volume while sparing normal tissue as much as possible. For photons, after a short energy deposit built-up region, the energy deposit decreased exponentially with depth. Unlike photons, ions exhibit inverse depth-dose profile. The energy deposit increases with increasing depth. After a plateau region at the entrance, there is a steep increase in energy deposition near the end of the range. This pronounced peak of energy deposition is known as Bragg peak in honor of W. H. Bragg [2]. By taking advantage of Bragg peak characteristics of ions, entrance dose and exit dose in charged particle therapy are greatly reduced. Depth-dose profiles of photon, proton and carbon ion are shown in Fig. 1.

This behavior of producing Bragg peak near the end of the range can be explained by the Bethe equation. As charge particle transverse through medium, it loses energy by Coulomb interaction with orbiting electrons and the nuclei. The dominant mechanism is interaction with orbiting electrons. This ionization energy loss by the projectile per unit length can be described by the Bethe equation Shell and density effect correction terms are neglected here. In Fig. 2, Bethe formula solved for proton and carbon ion is illustrated.

$$\frac{dE}{dx} = \rho \frac{4\pi r_0^2 N_A Z_t}{A_t} \frac{m_0 c^2 Z^2}{\beta^2} \left[ln \frac{2m_0 c^2 \beta^2}{I(1-\beta^2)} - \beta^2 \right]$$

[1] Master Student, Department of Physics, University of Mandalay.

[2] Professor, Dr., Department of Physics, University of Mandalay.

where r_0 is classical electron radius, $N_A$is Avogadro number, Z_t and Z are charge of target medium and projectile respectively, A_t is mass number of target medium, m_0 is rest mass of electron, $\beta = {}^{v}/_{c}$, v is velocity of projectile, c is velocity of light in vacuum and I is mean excitation of target medium in eV. The dependence of dE/dx on projectile's energy and charge could be seen from Fig. 2. At very high energy, thousand MeV range, there is nearly flat plateau region. As the particle gets slower, there is a steep increase in ionization energy loss. The ionization energy is at its maximum value just before the particle goes to stop. As the particle gets slower that its velocity is comparable to speed of orbiting electron, charged ions start picking up electrons. This causes decrease of net charge value and hence decrease in ionization energy loss. The dependence of net charge on the particle speed is given by the Barka's empirical formula [4].

$$Z_{eff} = Z\left[1 - exp(-125\beta Z^{2/3})\right]$$

Integrating dE/dx Vs Energy curve gives range-energy relationship. By using different energy of projectile, Bragg peak at different location is achieved.

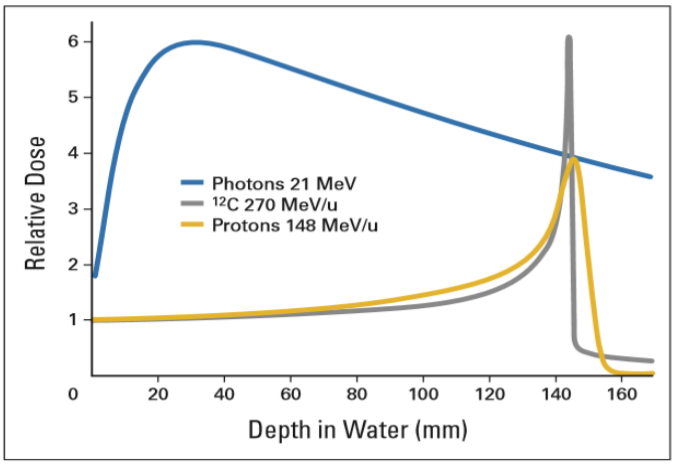

Fig. 1 Depth-dose profiles of photon, proton and carbon ion. Target material is water. Depth-dose curves of photon and proton are normalized so that they contribute same dose at 145mm. For same entrance dose as proton, carbon ion shows sharper Bragg peak. Figure from Schulz-Ertner and Tsujii [2].

Although the dominant mechanism is the interaction with orbiting electrons, they experience elastic Coulomb interactions with the atomic target nuclei. As a result of multiple Coulomb scattering events, deviation of charged particle projectile from its initial path direction is observed. Deflection from its initial beam direction of projectile charge particle due to this multiple Coulomb scattering events leads to lateral broadening of the beam. For different energies corresponding to similar penetration depths, lighter ions experience the lateral deflection than heavier ions. So, heavier carbon ions show better focused pencil beam at certain depth position.

Another effect that governs beam characteristic is range straggling or energy straggling. Range straggling is defined as the fluctuation in range from mean range value for each particle. This fluctuation in range is due to the statistical nature of interaction of charge particle with target nuclei. This effect causes Bragg peak little wider. For range straggling effect, it is inversely proportional to the square-root of the mass [5]. Therefore, heavier carbon ion has much stepper Bragg peak with sharp distal fall-off Bragg peak in compared with proton. But the interaction of carbon ion with target nuclei causes the fragmentation of the projectile into lighter particles (H, He, Li, Be, B). Since the dependence of ionization energy loss on Z^2, those lighter particles travel far beyond the Bragg peak and contribute the exist dose tail beyond Bragg peak. These lighter fragmented nuclei contribute dose to the normal healthy tissue outside the targeted tumor volume, making broadening the radiation field and hence increase the risk of forming

secondary tumors in surrounding normal tissue. In this paper, lateral dose due to multiple Coulomb scattering effect and distal dose for proton and carbon ions due to fragmentation effect are compared by using PHITS code [6].

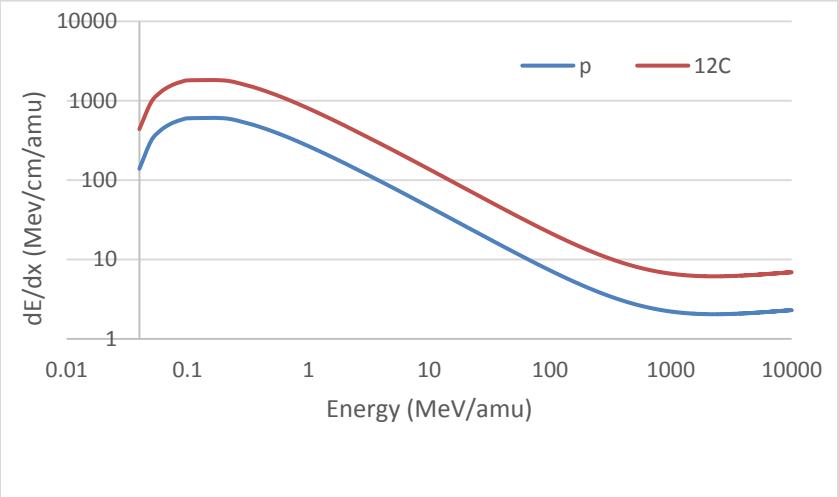

Fig. 2 Bethe equation solved for proton and carbon ion beam. Target material is water phantom. X-axis represents Energy per amu. Y-axis represents ionization energy loss divided by mass number. For ionization energy loss of carbon ion, Y-axis value must be multiplied with mass number of carbon ion, 12.

Computation Details

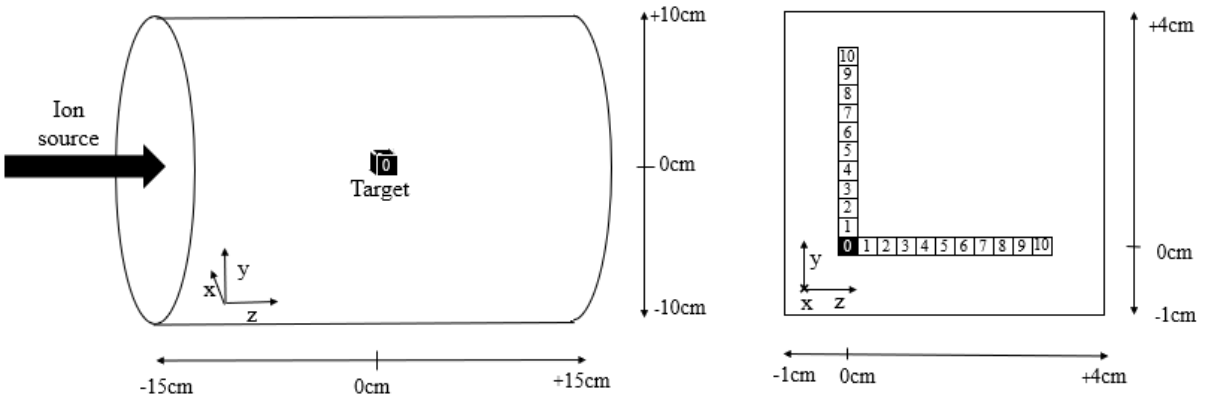

Fig. 3 (a) 3D view of constructed geometry and (b) Enlarged view of part of cylinder region on YZ plane. Box no.0 is targeted volume. Extra boxes are located along vertical Y-axis and along horizontal Z axis. All boxes are situated on the same YZ plane.

To compare lateral dose and distal dose contributed by proton and carbon, Monte Carlo simulations are performed by using PHITS code, version (3.17). In simulations, proton of energy 157.6MeV/u and carbon of energy 299.5MeV/u were delivered to the phantom which is composed of tissue-equivalent material A-150 plastics. For each ion beam, the lateral size is 3mm width. The geometry used for each simulation is shown in Fig. 1. The phantom has dimensions of radius 10cm and length 30cm. The dark box located at the center (0,0,0) is targeted volume. Extra boxes sitting along vertical Y-axis and horizontal Z-axis are

constructed to compare lateral dose and distal dose respectively. Dimension of each cube box is 3×3×3 mm^3.

Results and Discussion

Fig. 4-5 is the simulated results of dose distributions for proton and carbon ion. For proton beam, it shows focused beam shape at a few centimeters' depth. As it travels deeper near the targeted volume, lateral scattering leads to beam broadening and lateral dose are deposited beside the targeted volume. Another characteristic, range straggling effect contributes dose to areas just behind the target. For carbon ions, well focused carbon pencil beam is observed at similar penetration depth as proton. Due to fragmentation of carbon into lighter particles, we could observe long fragmentation tail behind the targeted volume, as expected.

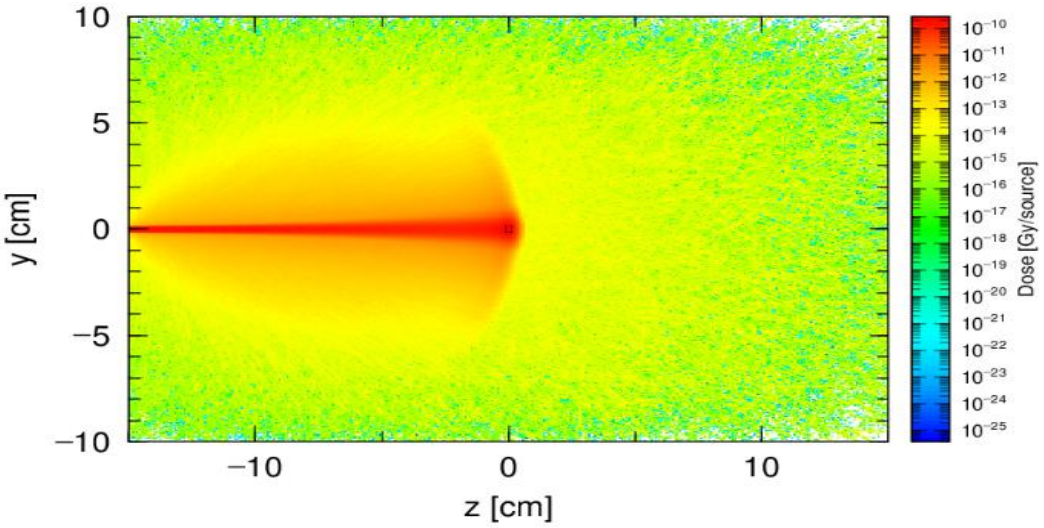

Fig. 4 2D view of dose profile for proton beam. Black box in the center is targeted volume.

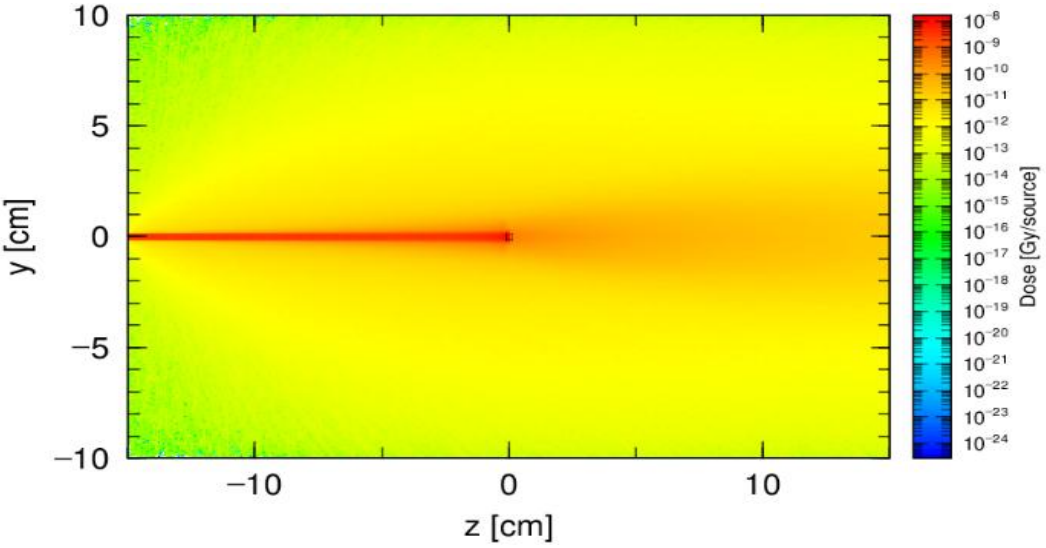

Fig. 5 2D view of dose profile for carbon beam. Black box in the center is targeted volume.

Fig 6 demonstrates relative energy deposit in targeted volume and boxes along Y-axis. Lateral dose comparison for proton and carbon beam could be observed. In the cell no.1, just next to the target, approximately 67% of the dose compared with the target dose is deposited for

proton beam while nearly just 13% for carbon beam. Energy deposit drops upper 1% in box number 4 (about 6mm away from targeted volume) for proton beam while the same effect happens in box no.2 (about 3mm away from targeted volume) for carbon beam. Minor lateral scattering is observed for carbon ion source.

Fig 7 represents relative energy deposit in targeted volume and boxes along Z-axis. Energy deposit in those extra boxes corresponds to distal dose behind target. For carbon ion, energy deposit in cell no.1 drops to 2.2% while 33% for proton beam. This is due to the sharp Bragg peak nature of carbon ion whereas wider Bragg peak for proton. Started from box no.2 (about 3mm behind targeted volume), energy deposit for proton beam drops under 1% abruptly. This is because proton does not undergo fragmentation process. For carbon ion, the distal dose does not quickly fall under 1% due to the lighter fragmented particles which travel beyond Bragg peak. Relative energy deposit in boxes are calculated by using PHITS code and output data are plotted in excel. Calculate data of Fig.6-7 are given in table 1.

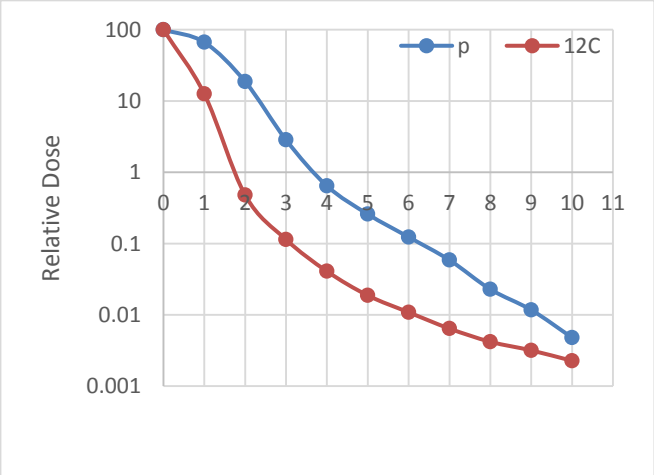

Fig. 6 Relative dose in targeted volume and boxes along vertical Y-axis. X-axis values on the graph represents box number in order. 0 is targeted volume. X-axis values 1-10 are boxes ordered from nearest to farthest distance from targeted volume.

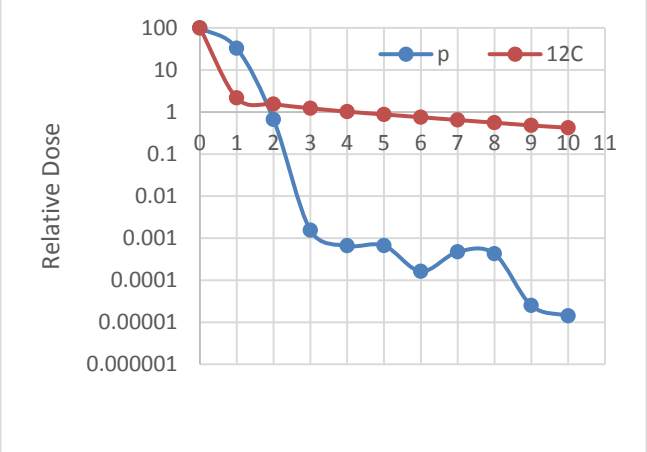

Fig. 7 Relative dose in targeted volume and boxes along horizontal Z-axis. X-axis values on the graph represents box number in order. 0 is targeted volume. X-values 1-10 are boxes ordered from nearest to farthest distance from targeted volume, similarly.

Table. 1 Calculated results of relative dose in extra boxes. Energy deposit in targeted volume is taken as reference point with value of 100.

Serial Number of boxes	Relative dose in boxes located along Y-axis		Relative dose in boxes located along Z-axis	
	proton source	carbon source	proton source	carbon source
1	66.612000	12.555710	32.772000	2.162925
2	18.686000	0.478875	0.663130	1.536038
3	2.844600	0.113991	0.001545	1.232308
4	0.644690	0.040857	0.000660	1.020978
5	0.258600	0.018717	0.000667	0.875194
6	0.123300	0.010861	0.000163	0.752779
7	0.058643	0.006414	0.000471	0.645368
8	0.022797	0.004192	0.000425	0.557554
9	0.011717	0.003172	0.000025	0.479732
10	0.004793	0.002264	0.000014	0.422839

Conclusion

In this paper, lateral dose and distal dose of proton and carbon ion beam sources are compared by calculating energy deposit in extra boxes of $3\times3\times3$ mm^3 dimensions. By comparing the energy deposit in boxes, carbon ion shows a tighter beam with minor lateral scattering and longitudinal straggling in compared with proton. As a result, we can conclude that carbon has better local control of energy which means any part of tumor could be irradiated with optical precision. But due to its fragmentation tail, it would be necessary to determine the energy contributed by those fragmentated ions beyond our targeted volume because organs at risk may be located behind tumor volume. The study of fragmented particles' yield and energy deposition due to these secondary particles is our future work.

Acknowledgement

We thank Professor Dr. Lei Lei Win and Dr. Kalar Thwe, Dr. Nay Win Oo, Physics Department, University of Mandalay, for their encouragement and permission.

References

[1] Wilson RR: Radiological use of fast protons. Radiology 47:498-491, 1946
[2] W. H. Bragg and R. Kleeman, Phil. Mag. 8 (1904) 726
[3] D.Schulz-Ertner and H.Tsujii, J. Clin. Oncol. 28, 8 (2007)
[4] Barkas, W. & Evans, D. Nuclear Research Emulsions: Techniques and Theory. Pure and applied physics (Academic Press, 1963).
[5] U. Linz, in: U. Linz (ed.), Ion Beams in Tumour Therapy, Chapman & Hall, London – Glasgow - Weinheim - New York - Tokyo - Melbourne Madras, 1995, 15
[6] https://phits.jaea.go.jp